RADIATIVE RECOMBINATION AND PHOTOIONIZATION OF HEAVY ELEMENT IMPURITIES IN PLASMAS

M. B. Trzhaskovskaya

Department of Theoretical Physics
Petersburg Nuclear Physics Institute, Gatchina 188300, Russia

V. K. Nikulin

Division of Plasma Physics, Atomic Physics, and Astrophysics
A.F.Ioffe Physical-Technical Institute, St.Petersburg 194021, Russia

R. E. H. Clark

Nuclear Data Section
International Atomic Energy Agency, Vienna A-1400, Austria

Research Co-ordination Meeting on CRP

"Atomic data for heavy element impurities in fusion reactors"

IAEA, Vienna, Austria, 4–6 March, 2009

Introduction

For a time after the last CRM, we performed the following studies.

1. *The unified database of the Radiative Recombination Cross Sections (RRCS) and Photoionization Cross Sections (PCS) for the heavy element impurity ions has been supplemented with 36 ions of Si, Cl, Ar, Ti, Cr, Kr, and Xe which are of importance in fusion studies.*

2. *We have studied the impact of relativistic and non-dipole effects on PCS, RRCS, and radiative recombination rate coefficients. The relativistic expression for the rate coefficient has been found.*

3. *Using the relativistic expression and taking into account all multipoles of the radiative field, we have calculated partial and total rate coefficients in a wide temperature range for highly-charged ions of tungsten which are of great current interest while the relevant data are not available.*

Results obtained throughout the course of performing our part of CRP have been presented in the following publications.

1. M.B. Trzhaskovskaya, V.K. Nikulin et al., "*Non-dipole second order parameters of the photoelectron angular distribution for elements Z=1-100 in the photoelectron energy range 1-10 keV*". At. Data Nucl. Data Tables **92**, 245 (2006).
2. M.B. Trzhaskovskaya, V.K. Nikulin, and R.E.H. Clark, "*Radiative recombination and photoionization cross sections for heavy element impurities in plasma: I. Tungsten ions. Theory*". PNPI Report, PNPI-2678, 36 p. (2006).
3. M.B. Trzhaskovskaya, V.K. Nikulin, and R.E.H. Clark, "*Radiative recombination and photoionization cross sections for heavy element impurities in plasma: II. Tungsten ions. Tabulated results*". PNPI Report, PNPI-2679, 53 p. (2006).
4. M.B. Trzhaskovskaya, V.K. Nikulin, and R.E.H. Clark, "*Radiative recombination and photoionization cross sections for heavy element impurities in plasmas: III. Ions of Iron, Nickel, and Copper. Tabulated results*". PNPI Report, PNPI-2699, 52 p. (2006).
5. M.B. Trzhaskovskaya, V.K. Nikulin, and R.E.H. Clark, "*Radiative recombination and photoionization cross sections for heavy element impurities in plasmas: IV. Molybdenum ions. Tabulated results*". PNPI Report, PNPI-2700, 28 p. (2006).
6. M.B. Trzhaskovskaya and V.K. Nikulin, *"Comment on "Quantitative x-ray photoelectron spectroscopy: Quadrupole effects, shake up, Shirley background, and relative sensitivity factors from a database of true x-ray photoelectron spectra"*. Phys.Rev.B **75**, 177104 (2007).

7. M.B. Trzhaskovskaya, V.K. Nikulin, and R.E.H. Clark, "*Radiative recombination and photoionization cross sections for heavy element impurities in plasmas*". At. Data Nucl. Data Tables **94**, 71 (2008).

8. M.B. Trzhaskovskaya, V.K. Nikulin, and R.E.H. Clark, "*Radiative recombination and photoionization cross sections for heavy element impurities in plasmas: II. Ions of Si, Cl, Ar, Ti, Cr, Kr, and Xe*". At. Data Nucl. Data Tables (accepted for publication).

9. V.I. Nefedov, V.G. Yarzhemsky, and M.B. Trzhaskovskaya, "*The influence of relaxation and nondipole effects on the intensity of X-ray photoelectron spectra*". Bull. Russian Acad. Sci.: Physics **72**, 423 (2008).

10. M.B. Trzhaskovskaya, V.K. Nikulin, R.E.H. Clark , "*Multipole and relativistic effects in radiative recombination process in hot plasmas*". Phys. Rev. E **78**, 035401 (R) (2008).

11. M.B. Trzhaskovskaya, V.K. Nikulin, and R.E.H. Clark, "*Radiative recombination rate coefficients for tungsten highly-charged ions*". At. Data Nucl. Data Tables (accepted for publication).

1. Photoionization and radiative recombination cross sections

Now the database contains the total RRCS and partial PCS for 67 ions. The cross sections are presented for more than 40 values of the kinetic electron energy in the range from the ionization threshold energy $\varepsilon_{n\kappa}$ to $E_k \lesssim 50$ keV. The calculations were carried out by the use of our computer code package RAINE [1, 2, 3]. A numerical accuracy of the PCS calculations is better than 0.1%.

Table 1. Charges of recombining ions

Configuration	Si	Cl	Ar	Ti	Cr	Fe	Ni	Cu	Kr	Mo	Xe	W
bare nucleus	14	17	18	22	24	26	28	29	36	42	54	74
H-like	13	16	17	21	23	25	27	28	35	41	53	73
He-like	12	15	16	20	22	24	26	27	34	40	52	72
Ne-like	4	7	8	12	14	16	18	19	26	32	44	64
Ar-like				4	6	8	10	11	18	24	36	56
"Ni-like"									8	14	26	46
Kr-like										6	18	38
Pd-like											8	28
"Er-like"												6

Note: the "Ni-like" configuration is $[\mathrm{Ar}]3d^4_{3/2}3d^6_{5/2}$; the "Er-like" one is $[\mathrm{Xe}]4f^6_{5/2}4f^8_{7/2}$

The Dirac-Fock (DF) method was applied where, as distinct from the Dirac-Slater (DS) method used in previous papers, the exchange interaction was taken into account exactly. PCS and RRCS obtained in the framework of the DF and DS methods may significantly differ, especially for low-charged ions. RRCS obtained within the DF and DS method for low-charged ions are shown in Fig. 1.

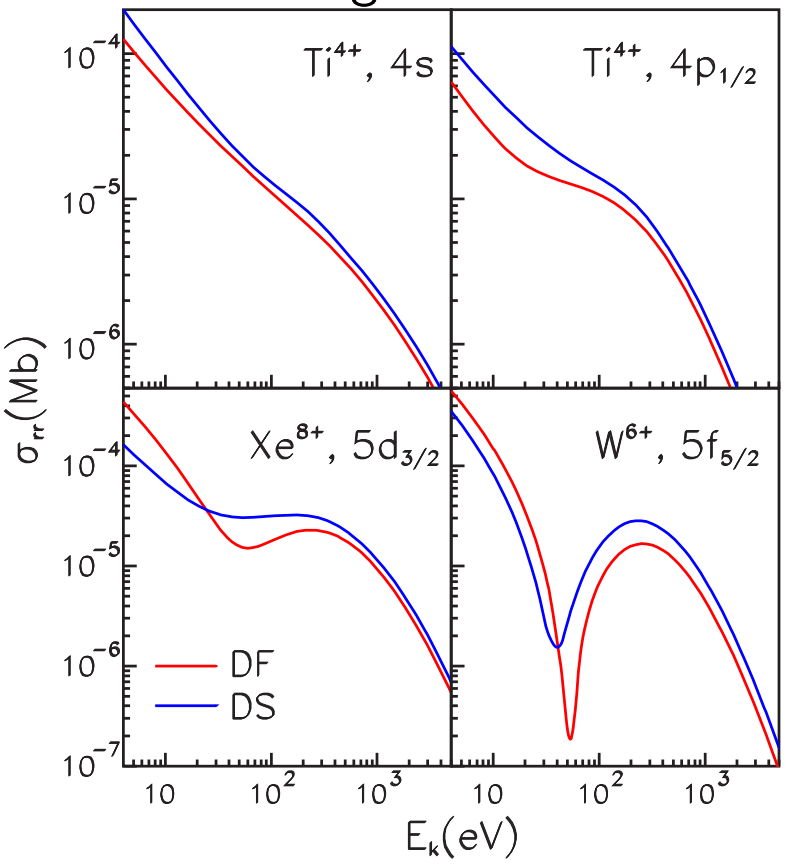

Figure 1: RRCS $\boldsymbol{\sigma_{rr}^{(n\kappa)}}$ (in Mb) versus the electron energy $\boldsymbol{E_k}$. Red, DF calculation; blue, DS calculation.

Table 2. Difference Δ_{DS} (in %) between subshell RRCS calculated by the use of the DF and DS models: $\Delta_{DS} = \left[\frac{\sigma_{rr}(DS)-\sigma_{rr}(DF)}{\sigma_{rr}(DF)}\right] \cdot 100\%$.

	Ti^{4+}		Xe^{8+}	W^{6+}
E_k, eV	$4s$	$4p_{1/2}$	$5d_{3/2}$	$5f_{5/2}$
10	44	92	-50	-45
109	18	30	71	116
1153	20	27	24	61
9646	22	33	29	69
31392	24	37	31	71
50327	24	37	31	71

As is seen, at a low electron energy, the difference Δ_{DS} is essential. Even at higher energies $E_k \gtrsim 30$ keV, differences between the DS and DF cross sections are also considerable — from 24% to 71% and kept constant. Due to such large differences in the RRCS and PCS values, the more accurate DF model should be preferred.

Summing subshell RRCS $\sigma_{rr}^{(n\kappa)}$ over all unfilled states, one arrives at the total RRCS

$$\sigma_{rr}^{tot} = \sum_{n=n_{\min}}^{\infty} \sum_{\kappa=\mp 1,\mp 2,\ldots,-n} \sigma_{rr}^{(n\kappa)} , \quad (1)$$

where $n_{\min}$ combined with the appropriate value of κ refers to the ground state of the recombined ion. An electron state is denoted by n and the relativistic quantum number $\kappa = (\ell - j)(2j + 1)$. As is well-known, the infinite series over n in Eq. (1) converges slowly. In a real plasma, however, there is a cutoff of bound levels from density effects. In particular, for fusion plasmas with electron density of the order of $10^{14}/cm^3$, the upper limit is $n \approx 20$. Because of this, the subshell PCS and RRCS were computed for the ground and all excited electron states with $n \leq 20$.

To minimize a great body of data, subshell PCS for states with $n \leq 12$ and orbital quantum number $\ell \leq 6$ were fitted by the following analytical expressions which was put forward by us earlier [4]

$$\sigma_{ph}^{(n\kappa)}(k) = \sigma_0 F(y) , \quad y = k/k_0 , \quad (2)$$

$$F(y) = \left[(y-1)^2 + y_w^2\right] y^{-Q} \left(1 + \sqrt{y/y_a}\right)^{-p} . \quad (3)$$

Here $k = E_k + \varepsilon_{n\kappa}$ is the photon energy, σ_0, k_0, y_w, y_a, and p are fit parameters, and $Q = 5.5 + \ell_{n\kappa} - 0.5p$. With Eqs. (2),(3), the fit parameters were obtained by minimizing the mean-square deviation from calculated values using the simplex search method [5].

To assess an accuracy of the fitting procedure, we found the relative root-mean-square error $\boldsymbol{\delta_{av}}$ as follows:

$$\boldsymbol{\delta_{av}} = \sqrt{\frac{1}{M}\sum_{i=1}^{M}\left[\frac{\sigma_{calc}^{(n\kappa)}(k_i) - \sigma_{fit}^{(n\kappa)}(k_i)}{\sigma_{calc}^{(n\kappa)}(k_i)}\right]^2} \cdot 100\%\,, \tag{4}$$

where $\boldsymbol{M}$ is the number of points involved in the fitting, $\boldsymbol{\sigma_{calc}^{(n\kappa)}(k_i)}$ and $\boldsymbol{\sigma_{fit}^{(n\kappa)}(k_i)}$ are PCS calculated and obtained in the fitting, respectively. Usually, the fit accuracy was good with $\boldsymbol{\delta_{av} \lesssim 2\%}$. However there exist some cases where the error may be greater and reach $\boldsymbol{\lesssim 10\%}$.

Fig. 2 shows that even non-monotone curves $\boldsymbol{\sigma_{ph}^{(n\kappa)}(k)}$ having deep Cooper minima may be fitted quite good. Note that the high $\boldsymbol{nf}$ shells of the W^{5+} ion refer to the worst-fitting cases.

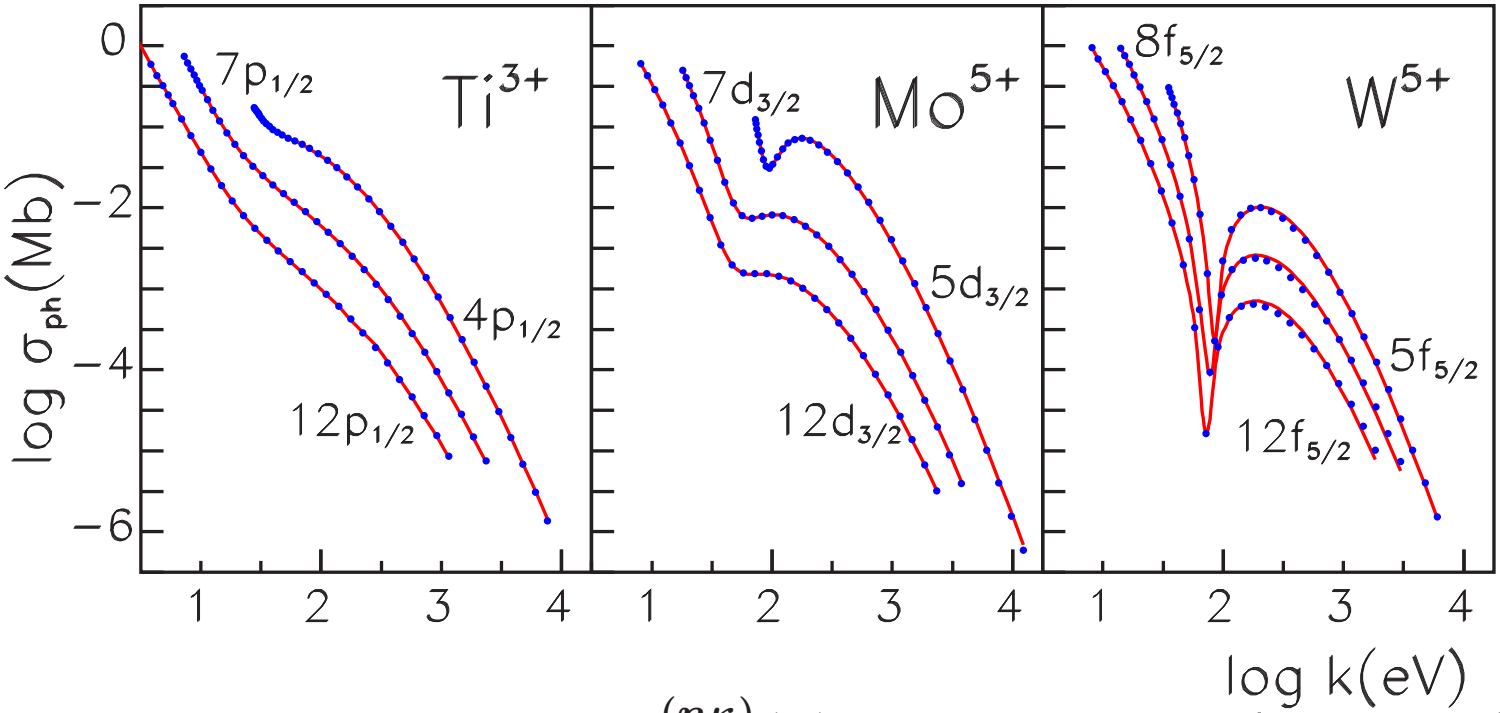

Figure 2: Fitting non-monotone curves $\boldsymbol{\sigma_{ph}^{(n\kappa)}(k)}$. PCS calculated (red curves) and fitted (blue circles) versus the photon energy $\boldsymbol{k}$.

Using the fit parameters from the database along with Eqs.(2) and (3), one can obtain PCS and RRCS at any photon energy from the energy range under consideration. By now, fit parameters for $\sim$ 7500 electron states were obtained and published.

2. The influence of relativistic and non-dipole effects

As is well known (see, for example, [3, 6, 7, 8]), the relativistic and non-dipole (multipole) effects are of great importance in consideration of photoionization and radiative recombination at high electron energies, especially for heavy and highly-charged ions. In particular, Ichihara and Eichler[6] noted that the difference between the relativistic calculation of RRCS with regard to all multipoles and the non-relativistic calculation within the dipole approximation for the $\boldsymbol{1s, 2p}$ and $\boldsymbol{3d}$ shells of uranium is 10-18% even at electron energy as low as $\boldsymbol{E_k}$=10 eV and may exceed an order of magnitude at $\boldsymbol{E_k}$=1000 keV.

Nevertheless, the multipole and relativistic effects are usually neglected in plasma calculations. For example, Nahar et al. [9] used the dipole approximation while energies to 100 keV were considered. The dipole approximation is also adopted in a recent paper by Badnell [10] where rate coefficients for $\boldsymbol{Z} \leq 54$ are presented. The highest electron energy under consideration equals $\sim$ 4000 keV for $\boldsymbol{Z} = 54$. The widely-used tables of hydrogenic recombination rate coefficients by Burgess [11] were calculated within the non-relativistic dipole approximation for temperatures up to $\boldsymbol{T} = \boldsymbol{\infty}$. As to relativistic effects, the majority of calculations [9, 10, 12, 13] were carried out using semi-relativistic corrections.

In our calculations, all relativistic and multipole effects are taken into consideration. Moreover, a new fully relativistic formula for the rate coefficient was obtained by a consistent way, that is, firstly, using the relativistic expression for PCS; secondly, the relativistic expression for the transformation coefficient from PCS to RRCS; and, finally, the relativistic Maxwellian distribution of continuum electrons instead of the non-relativistic distribution adopted in all previous calculations.

2.1. Relativistic effects

The relativistic PCS including all multipoles can be written as

$$\sigma_{ph}^{(n\kappa)}(k) = \frac{4\pi^2\alpha}{k(2j_{n\kappa}+1)} \sum_{L} \sum_{\kappa} \Big[(2L+1) Q^2_{LL}(\kappa) + L Q^2_{L+1L}(\kappa) + (L+1) Q^2_{L-1L}(\kappa) - 2\sqrt{L(L+1)}\, Q_{L-1L}(\kappa) Q_{L+1L}(\kappa) \Big] . \quad (5)$$

Here α is the fine structure constant, L is the multipolarity of the radiative field, and $Q_{\Lambda L}(\kappa)$ is the reduced matrix element. Both bound and continuum wave functions are calculated in the self-consistent DF field of the corresponding ions with $N+1$ and N electrons, respectively.

The partial RRCS for the subshell $n\kappa$ is expressed as follows

$$\sigma_{rr}^{(n\kappa)} = A q_{n\kappa} \sigma_{ph}^{(n\kappa)} \tag{6}$$

where $q_{n\kappa}$ is the number of vacancies in the $n\kappa$ subshell prior to recombination. The transformation coefficient A can be derived from the principle of the detailed balance. The exact relativistic expression for the coefficient has the following form [3, 6]

$$A_{rel} = \frac{k^2}{2m_0c^2E_k + E_k^2}. \tag{7}$$

However in the majority of calculations [9, 10, 12, 14, 15, 16], the coefficient is used in the form obtained in the non-relativistic approximation

$$A = \frac{k^2}{2m_0c^2E_k}. \tag{8}$$

The difference between $\sigma_{rr}^{(n\kappa)}$ obtained with Eq. (7) and Eq. (8) depends on the electron energy E_k only and can be written as

$$\frac{\sigma_{rr}^{(n\kappa)}(A) - \sigma_{rr}^{(n\kappa)}(A_{rel})}{\sigma_{rr}^{(n\kappa)}(A_{rel})} = \frac{E_k}{2m_0c^2}. \tag{9}$$

As is evident, the difference is equal to $\lesssim 10\%$ at $E_k \leq 100$ keV but reaches $\sim 100\%$ at 1000 keV.

The relativistic recombination rate coefficient $\alpha_{rel}^{(n\kappa)}(T)$ can be found using the thermal average over the fully relativistic RRCS, the continuum electron velocity being described by the relativistic Maxwell-Jüttner distribution function $f(E)$ normalized to unity [17]

$$f(E)dE = \frac{E(E^2-1)^{1/2}}{\theta e^{1/\theta} K_2(1/\theta)} \times e^{-(E-1)/\theta} dE. \tag{10}$$

Here E is the total electron energy in units of m_0c^2 including the rest energy, $\theta = k_\beta T/m_0c^2$ is the characteristic dimensionless temperature, k_β is the Boltzmann constant and T is the temperature. The function K_2 denotes the modified Bessel function of the second order. Taking into account the relativistic distribution (Eq.(10)) along with the relativistic transformation coefficient A_{rel} (Eq.(7)), we found [18] an expression for the relativistic rate coefficient in the factorized form as follows

$$\alpha_{rel}^{(n\kappa)}(T) = < v\sigma_{rr}^{(n\kappa)} > = F_{rel}(\theta) \cdot \alpha^{(n\kappa)}(T). \tag{11}$$

Here $v = (p/E)c$ is the electron velocity with the momentum $p = \sqrt{E^2-1}$ and $\alpha^{(n\kappa)}(T)$ is similar to the recombination rate coefficient with the non-relativistic

Maxwell-Boltzmann electron distribution which may be written as [19]

$$\alpha^{(n\kappa)}(T) = (2/\pi)^{1/2} c^{-2} (m_0 k_\beta T)^{-3/2} q_{n\kappa} \int_{\varepsilon_{n\kappa}}^{\infty} k^2 \sigma_{ph}^{(n\kappa)}(k) e^{(\varepsilon_{n\kappa}-k)/(k_\beta T)} dk. \tag{12}$$

In Eq. (12), $F_{rel}(\theta)$ is the relativistic factor which has the form

$$F_{rel}(\theta) = \sqrt{\frac{\pi}{2}\theta} \Big/ K_2(1/\theta) e^{1/\theta}. \tag{13}$$

This is just the factor which has been disregarded in all previous calculations.

It follows from Eq. (13) that the relativistic factor for the recombination rate coefficient depends on temperature only. Adopting the relativistic distribution of continuum electrons results in a decrease of the rate coefficient by a factor of 1.2 at temperature $k_\beta T$ = 50 keV and up to a factor of 7 at $k_\beta T$ = 1000 keV. The T-dependence of the factor is demonstrated in Fig. 3. As is seen, the factor $F_{rel}(\theta)$ differs noticeably from unity beginning with several tens of keV.

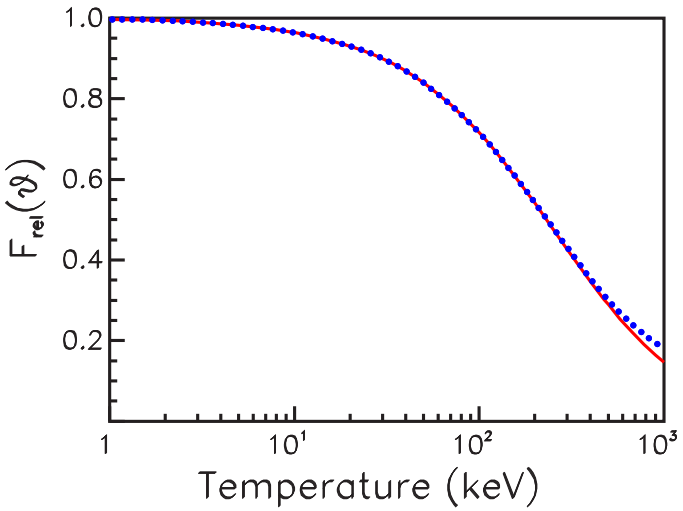

Figure 3: The exact relativistic radiative recombination rate coefficient factor $\boldsymbol{F_{rel}(\theta)}$ (red solid) and the approximate factor $\boldsymbol{\tilde{F}_{rel}(\theta)}$ (blue dotted).

One may easily obtain an approximate expression for the relativistic factor $\boldsymbol{F_{rel}(\theta)}$ using the asymptotic expansion of the Bessel function $\boldsymbol{K_2(1/\theta)}$ at large $\boldsymbol{1/\theta}$ [20], that is, at low temperature. The approximate expression can be written as

$$\boldsymbol{\tilde{F}_{rel}(\theta) = 1 \Big/ \left(1 + \frac{15}{8}\theta + \frac{105}{128}\theta^2 + ...\right).} \tag{14}$$

Eq. (14) provides an excellent approximation for $\boldsymbol{F_{rel}(\theta)}$. Comparison between the exact factor $\boldsymbol{F_{rel}(\theta)}$ and the approximate one $\boldsymbol{\tilde{F}_{rel}(\theta)}$ in Fig. 3 , reveals a very little difference

between the two curves: $\sim 4\%$ at $k_\beta T = 500$ keV and 25% at $k_\beta T = 1000$ keV.

To gain a better illustration, we display in Fig. 4 the rate coefficients obtained with and without regard to the factor $F_{rel}(\theta)$ for recombination of the $2s$ electron with the He-like ion of Xe. We see that the inclusion of the relativistic factor changes $\alpha^{(2s)}(T)$ considerably at high temperatures.

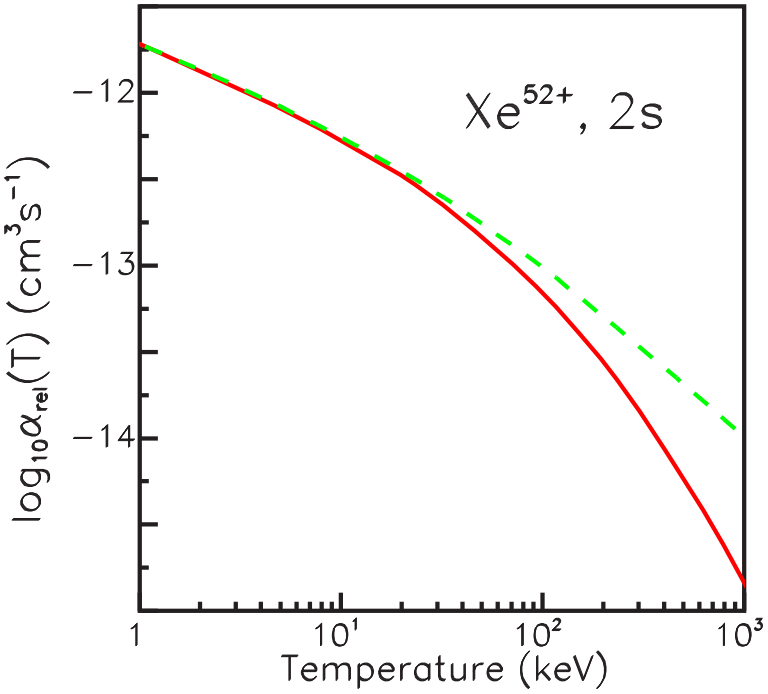

Figure 4: Rate coefficients $\alpha^{(2s)}(T)$ with (red) and without (green) regard to the relativistic factor $F_{rel}(\theta)$ for recombination of the $2s$ electron with the Xe^{52+} ion.

2.2. Non-dipole effects

To assess the impact of non-dipole effects, that is multipoles with $L > 1$, let us compare calculations in the dipole approximation with those including all multipoles. As is shown, red and blue curves diverge noticeably even at several keV. At the highest energy 1000 keV, in the case of W^{74+}, σ_{rr}(dip) is smaller than the exact value σ_{rr}(L) by a factor of $\sim$5 for the $1s$ shell and by a factor of $\sim$40 for the $4f_{5/2}$ subshell.

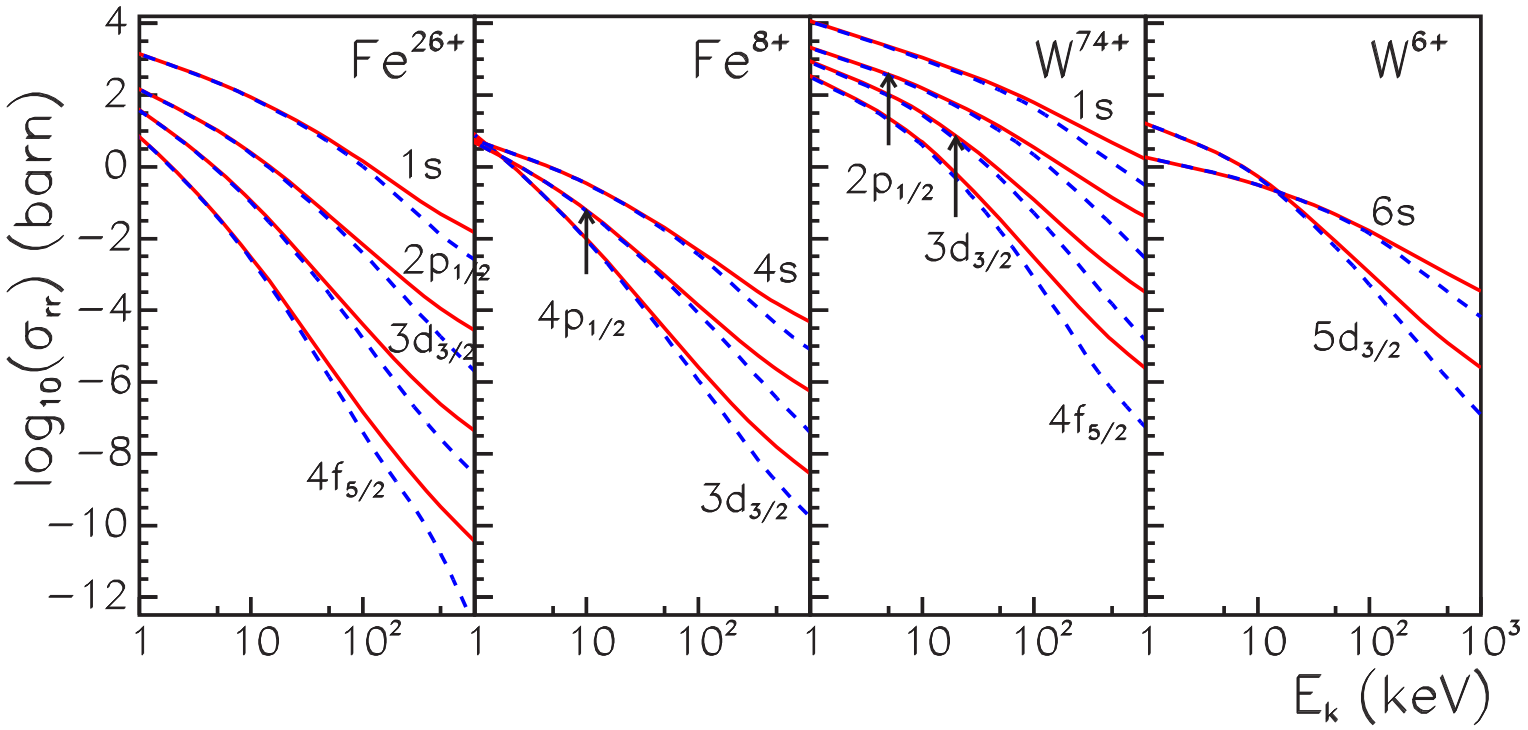

Figure 5: RRCS calculated including all multipoles L (red) and within the dipole approximation (blue).

Table 3. Difference Δ_{dip} (in %) between RRCS calculated taking into account all multipoles σ_{rr}(L) and within the dipole approximation σ_{rr}(dip) for bare nuclei

E_k,	$1s$ shell				$2p_{1/2}$ shell				$3d_{3/2}$ shell				$4f_{5/2}$ shell			
keV	Ne	Fe	Xe	W	Ne	Fe	Xe	W	Ne	Fe	Xe	W	Ne	Fe	Xe	W
0.01	0.1	0.7	2.9	5.2	0.1	0.7	2.6	4.3	0.1	0.6	2.5	4.5	0.1	0.6	2.5	4.6
1	0.4	1.0	3.2	5.4	0.7	1.2	3.1	4.8	1.1	1.6	3.5	5.5	1.7	2.2	4.0	6.0
10	3.2	3.8	5.8	7.9	5.6	6.2	7.7	8.9	10	10	12	13	15	15	16	18
50	15	15	17	18	24	24	25	24	38	38	38	38	51	52	52	52
100	27	27	28	29	40	40	40	39	58	58	57	57	75	73	73	73
500	75	74	74	72	84	84	84	82	89	89	90	90	97	95	95	95
1000	83	83	82	82	92	93	93	93	93	94	95	95	98	97	97	98

As is shown from Table 3, the dipole approximation differs from the exact calculation by $\sim \mathbf{3-20\%}$ at E_k=10 keV, $\sim \mathbf{15-50\%}$ at E_k=50 keV, and $\sim \mathbf{100\%}$ (by several multiples in reality) at E_k=1000 keV. The dependence of Δ_{dip} on the orbital quantum number $\ell_{n\kappa}$ of the shell under consideration is shown to be noticeable, Δ_{dip} being larger with increasing $\ell_{n\kappa}$. The difference Δ_{dip} depends slightly on Z as well as the difference is scarcely affected by the ion charge and the principal quantum number of the shell.

Let us consider the difference $\boldsymbol{\Delta_\alpha = [[\alpha^{(n\kappa)}_{rel}(L) - \alpha^{(n\kappa)}_{rel}(dip)]/\alpha^{(n\kappa)}_{rel}(L)] \cdot 100\%}$ for recombination of the $\boldsymbol{2s, 2p_{1/2}, 3s, 3p_{1/2},}$ and $\boldsymbol{3d_{3/2}}$ electrons with the He-like ions. These electron states are the lowest excited ones. As is evident, the difference $\boldsymbol{\Delta_\alpha}$ is more considerable for heavy elements. The inclusion of higher multipoles may change partial rate coefficients by $\sim 7\%$ at temperature $\boldsymbol{T = 10^8}$ K, by $\sim 20\%$ at $\boldsymbol{T = 10^9}$ K, and by $\sim 50\%$ at $\boldsymbol{T = 10^{10}}$ K for W^{72+}.

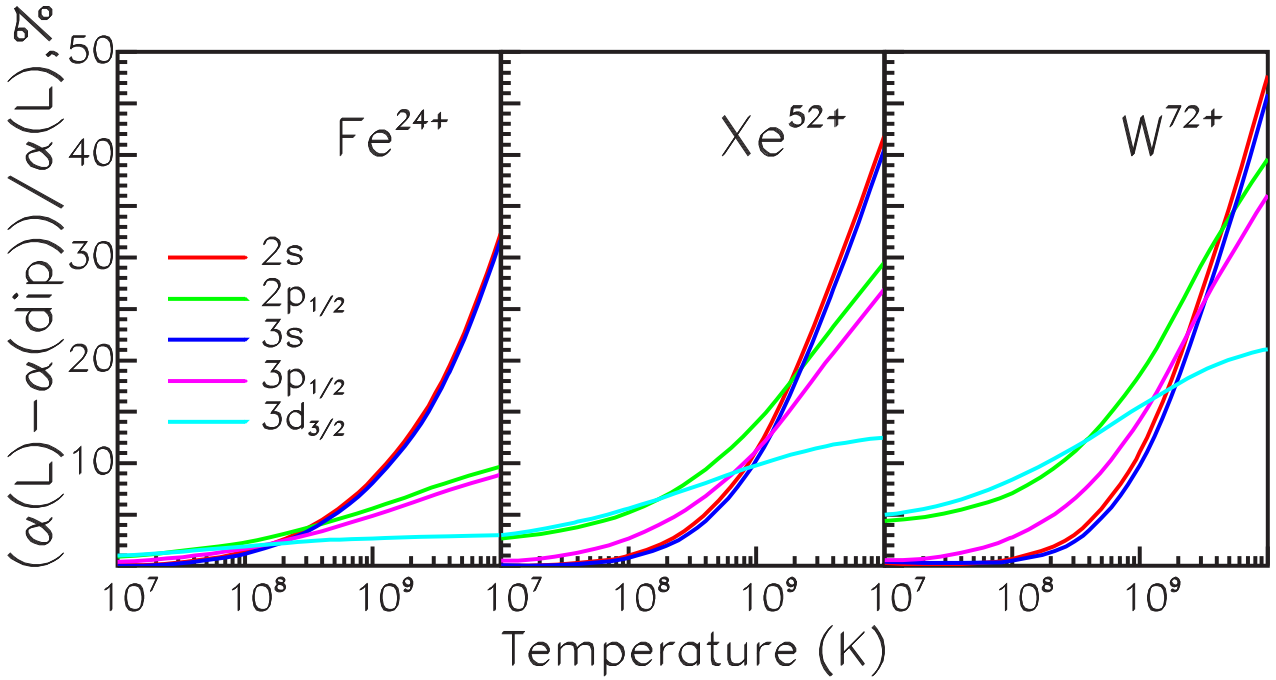

Figure 6: Difference $\boldsymbol{\Delta_\alpha}$ between rate coefficients calculated including all multipoles and in the dipole approximation for recombination of the lowest excited electron states with the He-like ions.

So, RRCS as well as rate coefficients obtained within the dipole approximation are inaccurate at high energies. Table 4 demonstrates how many multipoles L must be taken into account for various shells of the ion W^{73+} to achieve the accuracy prescribed in our PCS calculations.

Table 4. A number of multipoles L taken into account for the W^{73+} ion

E_k, keV	$1s$	$2p_{1/2}$	$3d_{3/2}$	$4f_{5/2}$
10	5	6	8	10
50	6	7	10	12
100	7	8	11	14
500	13	16	21	26
1000	19	24	31	37

As is seen, a number of multipoles is vastly larger than unity.

2.3. Asymptotic values of photoionization cross sections at high energy

Another problem in the rate coefficient calculation is concerned with the necessity to involve PCS or RRCS at high electron energy. Because the proper PCS calculation at high energy is a difficult task, many authors match asymptotic values. Usually the well-known asymptotic expression is involved [10, 15] which has been derived in the framework of the non-relativistic dipole approximation and can be written as follows [21, 22]

$$\sigma_{ph}^{(n\kappa)} \sim k^{-(3.5+\ell_{n\kappa})}. \tag{15}$$

However, Eq. (15) breaks down for the asymptotic behavior of the relativistic PCS with regard to all multipoles L. Let us consider the product $\sigma_{ph}^{(ns)} \times k^{3.5}$ for the s-shells. If the PCS asymptotic behavior (15) holds, the product has to be a constant. The DF calculations of $\sigma_{ph}^{(ns)}$ were carried out with allowance made for all L (solid) and within the electric dipole approximation (dashed). As is seen, solid curves increase in the whole photon energy range at $m = 3.5$ (Figs. 7(a) and 7(b)). The dashed (dipole) curves are something like an approximate constant at the photon energy $k \approx$ 100-150 keV. However at higher energies they increase also.

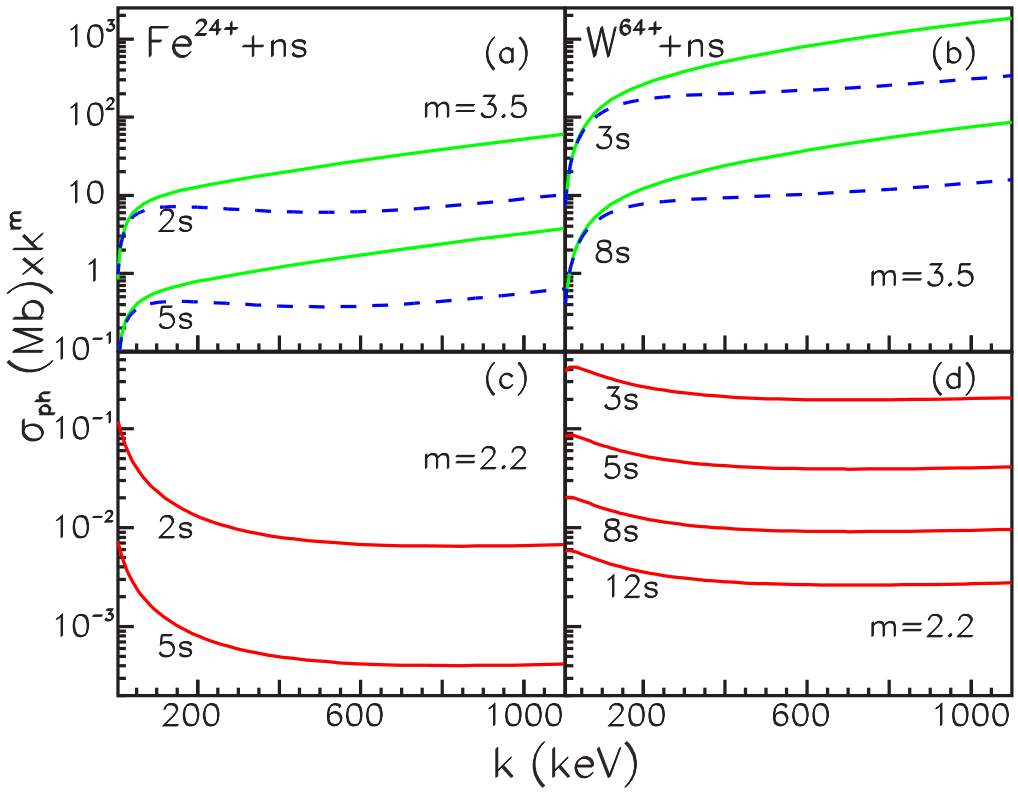

Figure 7: Photoionization cross sections $\sigma_{ph}^{(ns)}(k)$ multiplied by k^m where $m = 3.5$ ((a) and (b)) and $m = 2.2$ ((c) and (d)) for the ns shells of the Fe and W ions. Solid, with regard to all multipoles L; dashed, the dipole approximation.

We found the approximate asymptote for the s-electrons in the relativistic and multipole case

$$\sigma_{ph}^{(n\kappa)} \sim k^{-2.2}. \tag{16}$$

The product $\sigma_{ph}^{(ns)} \times k^{2.2}$ becomes a constant at energies $k \approx$ 500-600 keV. Eq.(16)

holds for various ns shells ($2 \leq n \leq 12$) as well as for different elements and ions.

However, a general expression for the PCS asymptotic behavior is unknown. So we found the values of $\sigma_{ph}^{(n\kappa)}$ with no any analytical asymptote by the direct DF calculations which were carried out up to the energy $E_k \approx 7000$ keV for the s, p, and d shells and to several hundred keV for shells with larger orbital momenta.

2.4. Comparison with other calculations

We compare our PCS calculations with the corresponding results by Ichihara *et al.* [6] and Badnell [10] for the $1s$ shell of the H-like ion Xe^{53+}. The case of an one-electron ion is particularly convenient for checking the influence of the higher multipoles and the method of calculation because the ion is free from any inter-electron interactions. Besides, for an one-electron ion, cross sections obtained in the velocity and length gauge coincide.

As is evident, our calculation is in excellent agreement in the wide range of electron energy 1 eV $\leq E_k \leq$ 6000 keV with the values from a relativistic calculation [6] where all multipoles L were included. As a rule, our values of $\sigma_{ph}^{(n\kappa)}$ coincide with an accuracy of three significant digits given in [6]. The maximum difference between the two calculations

is $\sim 1\%$ at the highest energy $E_k = 6000$ keV.

Table 5. Comparison of our PCS calculation with results by Ichihara *et al.* [6] and by Badnell [10] for the $1s$ shell of the H-like ion Xe^{53+}

	σ_{ph}, Mb			σ_{ph}, Mb		
E_k, keV	Ichihara *et al.*	present	E_k, keV	Badnell	present	Δ, %
0.001	1.94(-3)	1.94(-3)	0.00083	2.246(-3)	1.937(-3)	-16
0.04	1.94(-3)	1.94(-3)	0.03967	2.240(-3)	1.935(-3)	-16
4.	1.52(-3)	1.52(-3)	3.967	1.734(-3)	1.523(-3)	-14
40.	3.08(-4)	3.08(-4)	39.67	3.256(-4)	3.114(-4)	-4.5
80.	9.94(-5)	9.94(-5)	83.31	9.095(-5)	9.206(-5)	1.2
200.	1.40(-5)	1.41(-5)	182.4	1.539(-5)	1.740(-5)	12
400.	2.75(-6)	2.75(-6)	396.7	1.894(-6)	2.802(-6)	factor 1.5
800.	5.97(-7)	5.97(-7)	833.1	2.071(-7)	5.495(-7)	factor 2.6
2000.	1.13(-7)	1.13(-7)	1824.	1.730(-8)	1.318(-7)	factor 7.6
4000.	4.07(-8)	4.07(-8)	3967.	1.350(-9)	4.117(-8)	factor 30
6000.	2.39(-8)	2.36(-8)				

By contrast, PCS obtained by Badnell exceed our values by $\sim 16\%$ in the energy range $E_k \lesssim 4$ keV and become smaller at higher energies, decreasing by approximately a

factor of 8 at $E_k \approx 1800$ keV and a factor of ~ 30 at $E_k \approx 4000$ keV. The comparison of our PCS $\sigma_{ph}^{(2s)}$ calculation with results by Badnell for comparatively light ion Fe^{23+} reveals the similar tendency, but smaller in magnitude at low energies. The reason of the difference at low energies is not quite clear for us. It is possible that this is the influence of methods of calculations used in [10]. However, the difference at higher energies is likely due to a combination of neglect of the higher multipoles and the semi-relativistic approximation used in [10].

Our total recombination rate coefficients for tungsten ions W^{74+}, W^{64+}, and W^{56+} were compared with the relativistic calculations by Kim and Pratt *et al.* [14] performed using a number of approximations (only few direct relativistic DS calculations of the RRCS, thereafter all other cross sections for each a state $n\kappa$ were obtained by interpolation using the quantum defect method). Although an approximate approach was used in [14], the comparison revealed a reasonable agreement between the two calculations. For example, the difference for bare nucleus ranged from 3% to 11% (depending on the temperature).

3. Radiative recombination rate coefficients for tungsten ions

There are only a few relativistic calculations of PCS and RRCS for ions of tungsten [6, 16]. As to the rate coefficients for tungsten ions, there are only the data by Kim and Pratt [14] for three ions obtained using an approximate theoretical method. The rates were calculated only at four values of temperature in the range 1 keV $\leq \boldsymbol{k_\beta T} \leq$ 30 keV. However, atomic data on tungsten ions are deeply involved in fusion studies, in particular, are important in the performance of future fusion devices developed in the framework of the tungsten program (see paper by R. Neu *et al.*, Nucl.Fusion, **45**, 209 (2005) [23]).

Because of this, we calculated the partial and total recombination rate coefficients for highly-charged ions of tungsten from the Pd-like ion W^{28+} to the bare nucleus W^{74+}. The wide range of temperatures $\mathbf{10^3}$ K$\leq \boldsymbol{T} \leq \mathbf{10^{10}}$ K (0.09 eV $\lesssim \boldsymbol{k_\beta T} \lesssim$ 900 keV) is considered. Relativistic DF calculations were performed using expressions and methods described above. The majority of the recombination rate coefficients were calculated with a numerical accuracy better than 1%, in the worst cases (outer shells and highest temperatures) the accuracy being $\lesssim \mathbf{5\%}$.

The database contains partial rate coefficients $\alpha_{rel}^{(n\kappa)}$ for electron states with $n \leq 12$ and $\ell \leq 6$ as well as the total recombination rate coefficients which are written as

$$\alpha_{tot} = \sum_{n\kappa} \alpha_{rel}^{(n\kappa)}. \tag{17}$$

The summation in Eq. (17) was extended over all electron states with $n \leq 20$. The partial rate coefficients included in the database contribute 70% - 99% into total rates.

We present the partial rate coefficients for so high electron shells because their magnitudes are sometimes comparable to those for lower shells. In Fig. 8, partial rate coefficients $\alpha_{rel}^{(n\kappa)}$ are shown versus the principal quantum number n for shells with various orbital momenta. The data are given for the ion W^{72+} and for the temperature $T = 10^7$ K (0.9 keV).

Though rate coefficients usually fall with increasing n, for shells with large ℓ, $\alpha_{rel}^{(n\kappa)}$ first increases with n (see the n-dependence of the g, h, and i shells). So that a number of shells with large n and ℓ contribute considerably to α_{tot}, especially at low temperature. A dependence of partial recombination rate coefficients on temperature is displayed in Fig. 9.

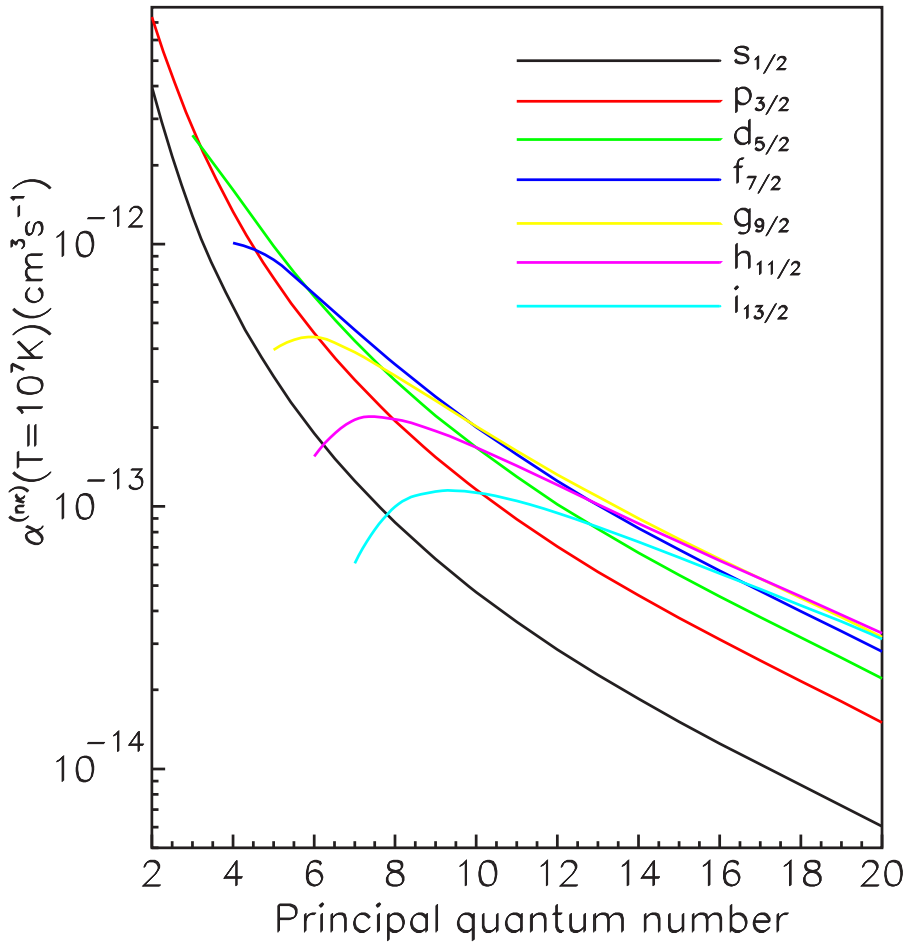

Figure 8: Partial rate coefficients $\boldsymbol{\alpha_{rel}^{(n\kappa)}}$ versus the principal quantum number $\boldsymbol{n}$ for recombination of various electrons with the ion W^{72+} at $\boldsymbol{T = 10^7}$ K.

It is seen that $\boldsymbol{\alpha_{rel}^{(n\kappa)}}$ for shells with large $\boldsymbol{\ell}$ are at times comparable with values for shells with smaller $\boldsymbol{\ell}$ or exceed them.

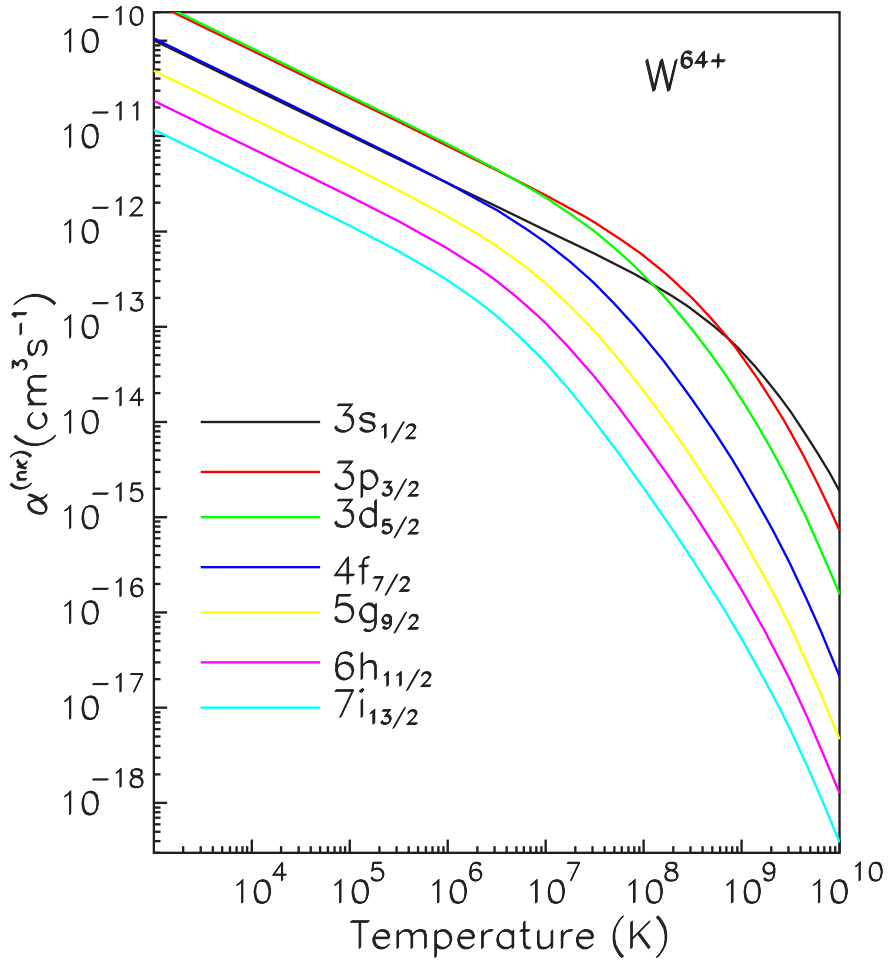

Figure 9: Partial rate coefficients $\alpha_{rel}^{(n\kappa)}$ versus temperature T for recombination of various electrons with the ion W^{64+}.

4. Conclusions

- Relativistic DF calculations of partial PCS and RRCS as well as total RRCS have been performed in the electron energy range from ionization thresholds to 50 keV for 67 ions of twelve elements which are of importance in fusion study. Partial PCS have been fitted by a simple analytical expression involving five fit parameters.

- We have calculated the relativistic DF partial and total rate coefficients in the wide temperature range $\mathbf{10^3}$ K $\leq \boldsymbol{T} \leq \mathbf{10^{10}}$ K for nine tungsten ions which are of great current interest and for which data are not available.

- For the first time, a new fully relativistic formula for the rate coefficient has been derived using the relativistic Maxwell-Jüttner distribution. The formula is factorized giving rise to the temperature-dependent relativistic correction factor for which the usual expression should be multiplied. The factor changes the rate coefficient considerably at a high energy.

- A contribution of non-dipole effects in rate coefficients has been shown to be significant (10-50%) at electron energies of the order of 10 keV and higher.

- The results obtained have been published in 11 papers.

References

[1] I.M. Band, M.B. Trzhaskovskaya, C.W. Nestor,Jr, P.O. Tikkanen, and S. Raman, Atomic Data and Nuclear Data Tables **81**, 1 (2002).

[2] I.M. Band, M.A. Listengarten, M.B. Trzhaskovskaya, and V.I. Fomichev. *Computer program complex RAINE*, I–VI, LNPI Reports LNPI-289 (1976); LNPI-298, LNPI-299, LNPI-300 (1977); LNPI-498 (1979); LNPI-1479(1989).

[3] M.B. Trzhaskovskaya and V.K. Nikulin, Optics and Spectroscopy **95**, 537 (2003).

[4] D.A. Verner, D.G. Yakovlev, I.M. Band, and M.B. Trzhaskovskaya, At. Data Nucl. Data Tables **55**, 233 (1993).

[5] D.M. Himmelblau, Applied Nonlinear Programming, McGraw-Hill, 1972, p. 163.

[6] A. Ichihara and J. Eichler, At. Data Nucl. Data Tables **74**, 1 (2000).

[7] M.B. Trzhaskovskaya, V.K. Nikulin, V.I. Nefedov, and V.G. Yarzhemsky, J.Phys. B: At. Mol. Opt. Phys. **34**, 3221 (2001).

[8] M.B. Trzhaskovskaya, V.I. Nefedov, and V.K. Nikulin, Atomic Spectroscopy **91**, 569 (2001).

[9] Sultana N. Nahar and Anil K. Pradhan, Radiation Physics and Chemistry **70**, 323 (2004).

[10] N.R. Badnell, Astrophys. J. Suppl. Series **167**, 334 (2006); available in http://amdpp.phys.strath.ac.uk/tamoc/DATA/PI/key.html.

[11] A. Burgess, Mem. Roy. Astron. Soc. **60**, Pt.1, 1 (1964).

[12] Sultana N. Nahar, Anil K. Pradhan, and Hong Lin Zhang, Astrophys. J. Suppl. Series, **133**, 255 (2001).

[13] Robert E.H. Clark, Robert D. Cowan and Frank W. Bobrowicz, At. Data Nucl.Data Tables **34**, 415 (1986).

[14] Young Soon Kim and R.H. Pratt, Phys. Rev. A **27**, 2913 (1983).

[15] D. A. Verner and G.J. Ferland, Ap. J. Suppl. **103**, 467 (1996).

[16] M.B. Trzhaskovskaya, V.K. Nikulin, and R.E.H. Clark, At. Data Nucl. Data Tables **94**, 71 (2008).

[17] Moorad Alexanian, Phys. Rev. **165**, 253 (1968).

[18] M.B. Trzhaskovskaya, V.K. Nikulin, and R.E.H. Clark, Phys. Rev. E **78**, 035401(R) (2008).

[19] W. D. Barfield, J. Phys. B: At. Mol. Opt. Phys. **13**, 931 (1980).

[20] *"Handbook of Mathematical Functions"*, ed. by M. Abramowitz and I.A. Stegun (National Bureau of Standards, Appl.Math.Series 5, 1964).

[21] U. Fano and J.W. Cooper, Rev. Mod. Phys. **40**, 441 (1968).

[22] H.A. Bethe and E.E. Salpeter, *"Quantum Mechanics of One- and Two-Electron Atoms"* (Springer-Verlag, Berlin, 1957) Chapter IV.

[23] R. Neu, R. Dux, A. Kallenbach *et al.*, Nucl.Fusion **45**, 209 (2005).

[24] Sultana N. Nahar and Anil K. Pradhan, Phys. Rev. A**49**, 1816 (1994).

[25] A.S. Kronrod, *"Nodes and Weights of Quadrature Formulas"* (Consultants Bureau, New York, 1965)